Chemical Science



PERSPECTIVE

View Article Online
View Journal | View Issue



Cite this: Chem. Sci., 2024, 15, 19212

dll publication charges for this article have been paid for by the Royal Society of Chemistry

Received 26th August 2024 Accepted 2nd November 2024

DOI: 10.1039/d4sc05707d

rsc li/chemical-science

Cationic Al oxo-hydroxide clusters: syntheses, molecular structures, and functional applications

Naoki Ogiwara, D Wei Zhou and Sayaka Uchida D*

Al oxo-hydroxide clusters, synthesized through the hydrolysis of Al³⁺ solutions, are expected to bridge the gap between metal-aqua complexes and bulk metal oxides/hydroxides. These clusters exhibit remarkable diversity in structure and composition, controlled by modulating the basicity of the solution and use of capping ligands. While anionic metal-oxo clusters, such as polyoxometalates, have been extensively studied since the early 20th century, cationic metal-oxo clusters, including those of aluminum, have gained interest more recently due to their high reactivity and potential for various applications. We explore their molecular structures and assembly into various forms, including ionic crystals, amorphous solids, and hybrid materials, for applications such as adsorption, coagulation, and catalysis. Furthermore, we present future perspectives, emphasizing molecular design, scalable synthetic methods, and expanded functional applications, particularly in energy and environmental sciences, where these clusters are expected to demonstrate significant potential.

1. Introduction

Metal-oxo clusters are broadly defined as inorganic multi-metal molecular complexes with aqua (H2O), hydroxide (OH-), or oxide (O²⁻) ligands.^{1,2} These clusters can be considered intermediate compounds that bridge the gap between metal-aqua complexes and metal oxides/hydroxides. They are expected to exhibit intrinsic physicochemical properties not observed in either metal-aqua complexes or metal oxides/hydroxides. Anionic metal-oxo clusters known as polyoxometalates (POMs) comprise group V or VI metals (V, Nb, Ta, Mo, W) and oxide ligands. POMs encompass extensive research areas, with their significance dating back to 1933 when Keggin reported the structure of [PW₁₂O₄₀]³⁻ through X-ray diffraction analysis.³⁻⁸ On the other hand, main group metals (Al, Sb, Bi, etc.), 9-14 group IV metals (Ti, Zr, Hf),15,16 or other metals (Fe, U, Np, etc.)17,18 with lower oxidation states and electronegativity form cationic metal-oxo clusters. These clusters often possess labile hydroxide and aqua ligands on their molecular surfaces, making crystallization more difficult. Consequently, due to their high reactivity, cationic metal-oxo clusters represent an emerging research field for functional applications.

Among the cationic metal–oxo clusters, aluminum (Al) oxohydroxide clusters have long been a subject of significant interest. Al, comprising about 8% by weight of the Earth's crust, is a typical metal prevalent in a wide variety of minerals. Aluminum oxides and hydroxides are widely used in applications such as adsorbents, heterogeneous catalysis, and coagulation processes. However, the compositions and

Department of Basic Science, School of Arts and Sciences, The University of Tokyo, Komaba, Meguro-ku, Tokyo, 153-8902, Japan. E-mail: csayaka@g.ecc.u-tokyo.ac.jp

structures of oxides (e.g., α , γ -type) and hydroxides (e.g., gibbsite, boehmite) are limited. Therefore, the use of clusters as components is expected to extend the compositions, structures, and functionalities of unexplored solid-state materials. Al species are present not only in the solid state but also in natural water systems, where Al3+ aqua ions hydrolyze, giving rise to a diverse array of Al oxo-hydroxide clusters. These clusters influence geochemical processes and soil chemistry, affecting Al floc formation in polluted streams and impacting bioavailability and phytotoxicity in ecosystems.24-26 They also hold potential for practical applications, including use as antiperspirants,27 anionic coagulants in water treatment,28 and precursors for fabricating thin film devices from aqueous solutions.29 In 2006, Casey reported a seminal review on cuttingedge research of Al oxo-hydroxide clusters at that time.9 Since the review's publication, the structural diversity of these clusters has increased, and molecular design strategies have been proposed, leading to the synthesis of metal-substituted Al oxohydroxide clusters and new applications, particularly in the solid state.

In this perspective, we aim to present the synthetic strategies for Al oxo-hydroxide-based clusters, focusing on designing their compositions and molecular structures. The assembly of these clusters for functional applications, such as adsorptive removal of pollutants and catalysis, will also be discussed.

2. Syntheses and molecular structures of Al oxo-hydroxide clusters

2.1 Al oxo-hydroxide clusters

Among Al oxo-hydroxide clusters, the Keggin-type $[Al_{13}O_4(-OH)_{24}(H_2O)_{12}]^{7+}$ (Al_{13}) structure is widely recognized as the most

well-known. In the Keggin-type Al₁₃, a central tetrahedral [AlO₄] unit is surrounded by four Al₃(OH)₆(H₂O)₃ trimers, and three rotational isomers $(\varepsilon, \delta, \gamma)$ of the Keggin-type Al_{13} has been successfully isolated. In 1960, Johansson and coworkers reported ε -Keggin-type Al_{13} (ε - Al_{13}) with T_d molecular symmetry (Fig. 1a), 30,31 in which the four surrounding Al₃(OH)₆(H₂O)₃ trimers are connected through edge-sharing of hydroxyl groups. ε-Al₁₃ was synthesized by thermal hydrolysis of an aqueous Al³⁺ solution, and in 1991, Nazar and coworkers found that thermal aging of ε-Al₁₃ in the presence of Na⁺ ions produced a new polycation, later identified as δ-Keggin-type Al₁₃ (δ-Al₁₃, Fig. 1b).32 In δ-Al₁₃, one of the four Al₃(OH)₆(H₂O)₃ trimers is rotated 60° relative to the remaining structure of ε-Al₁₃.³³ δ-Al₁₃ possesses C_{3v} molecular symmetry, and the average bond distance of tetrahedral [AlO₄] unit of δ -Al₁₃ is 1.80 Å, which is shorter than that of ε -Al₁₃ (1.83 Å). In 2013, Pan and coworkers reported γ -Keggin-type Al_{13} (γ - Al_{13} , Fig. 1c), in which two of the four Al₃(OH)₆(H₂O)₃ trimers are rotated 60° relative to the remaining structure of ϵ -Al₁₃.³⁴ The formation of γ -Al₁₃ was

achieved through the thermal hydrolysis of an Al³⁺-containing solution in the presence of Ca(OH)₂ and glycine. ¹H diffusionordered spectroscopy (DOSY) and ²⁷Al NMR data indicate that glycine binds to the Al_{13} isomers, suggesting that this binding is a crucial step in the isomerization process.³⁵ The authors propose that glycine serves as a buffer during the initial addition of base, preventing nonspecific hydrolysis by weakly and reversibly binding to Al³⁺ species. They also suggest that Ca²⁺ ions are essential in enabling the stepwise rotation of the trimeric subunits during this process. The molecular symmetry of γ -Al₁₃ is categorized as $C_{2\nu}$, and the average bond distance of the tetrahedral [AlO₄] unit of γ -Al₁₃ (1.78 Å) is shorter than that of ε-Al₁₃ (1.83 Å) and δ-Al₁₃ (1.80 Å). In 2016, Cheong, Pan, Casey, and coworkers observed a peak at 72 ppm in the ²⁷Al NMR spectra of thermally aged ε -Al₁₃ solution in the presence of glycine and CaCl2, which differed from the peak positions of tetrahedral Al in ε -Al₁₃ or δ -Al₁₃, indicating the presence of a different rotational isomer,35 while the attempts for isolation were unsuccessful.

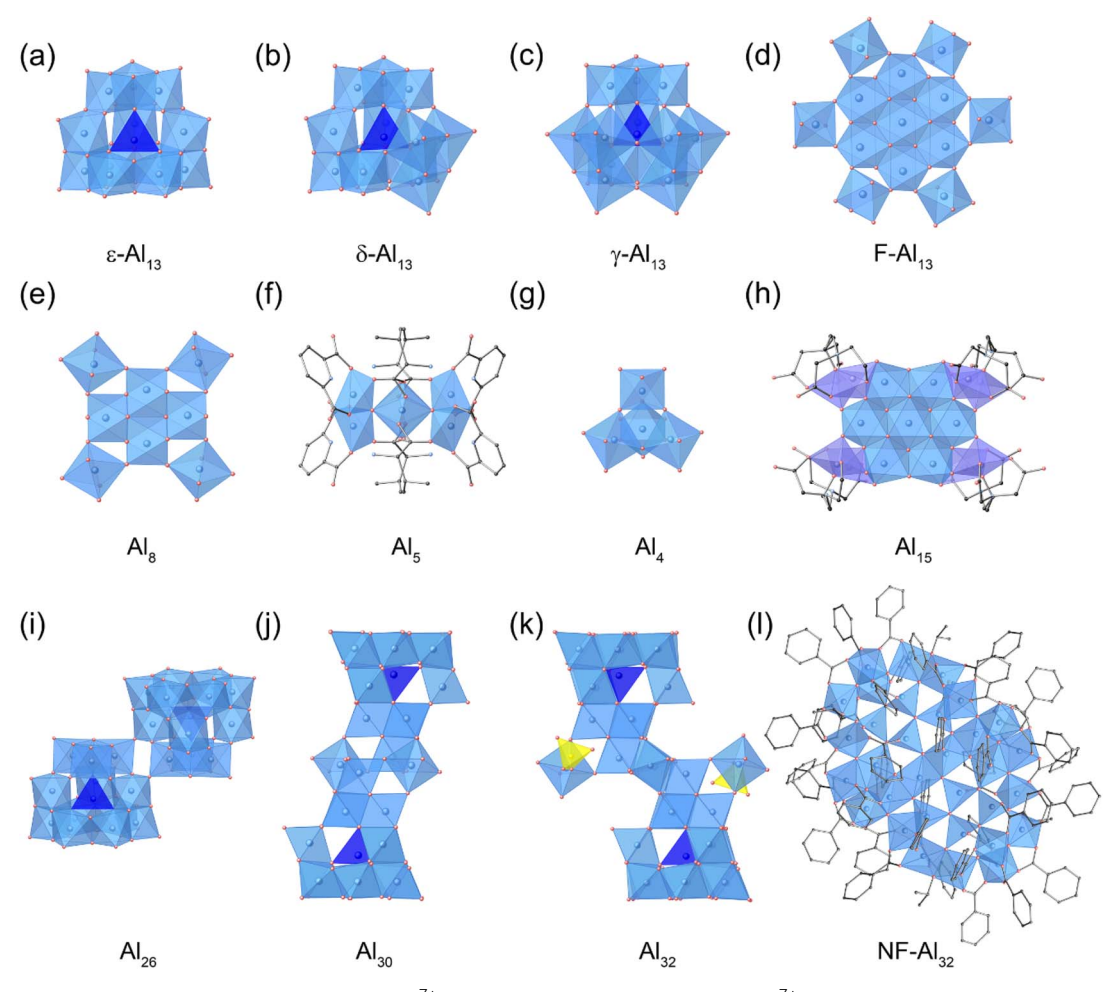


Fig. 1 Molecular structure of (a) $[\epsilon-Al_{13}O_4(OH)_{24}(H_2O)_{12}]^{7^+}$ $(\epsilon-Al_{13})$, (b) $[\delta-Al_{13}O_4(OH)_{24}(H_2O)_{12}]^{7^+}$ $(\delta-Al_{13})$, (c) $[\gamma-Al_{13}O_4(OH)_{24}(H_2O)_{12}]^{7^+}$ $(\gamma-Al_{13})$, (d) $[Al_{13}(OH)_{24}(H_2O)_{24}]^{15^+}$ $(F-Al_{13})$, (e) $[Al_8(OH)_{14}(H_2O)_{18}]^{10^+}$ (Al_8) , (f) $[Al_5O_2(OH)_2(HPDA)_4(L-Val)_4]^+$ (Al_5) , (g) $[Al_4(OH)_6(H_2O)_{12}]^{6^+}$ (Al_4) , (h) $[Al_{15}O_4(OH)_{20}(hpdta)_4]^{3^-}$ (Al_{15}) , (i) $[Al_{26}O_8(OH)_{50}(H_2O)_{20}]^{12^+}$ (Al_{26}) , (j) $[Al_3O_8(OH)_{56}(H_2O)_{26}]^{18^+}$ (Al_{30}) , and (k) $[Al_{32}O_8(OH)_{60}(H_2O)_{28}(SO_4)_2]^{16^+}$ (Al_{32}) , (l) $[Al_{32}(benzoate)_{36}(O^7Pr)_4(\mu_3-O)_{24}(\mu_4-O)_4]$ $(NF-Al_{32})$. $[AlO_6]$, $[AlO_4]$ and $[SO_4]$ are shown by the light blue, dark blue, and yellow polyhedrons, respectively.

Chemical Science

In 1995, Heath and coworkers carried out the thermal hydrolysis of an agueous Al³⁺ solution with N-(2-hydroxyethyl) iminodiacetic acid (H₃heidi = HOCH₂CH₂N(CH₂COOH)₂) and discovered the formation of a flat-shaped Al₁₃ cluster composed entirely of octahedral [AlO₆] units ([Al₁₃(μ_3 -OH)₆(μ_2 -OH)₁₂(heidi)₆ $(H_2O)_6$]³⁺, **F-Al**₁₃·heidi). ³⁶ In **F-Al**₁₃·heidi, an [AlO₆] core is surrounded by six additional [AlO₆] units connected *via* μ₃-OH bridges, creating a coplanar configuration. Six more [AlO₆] octahedra are alternately attached above and below the primary plane through shared oxygen vertices. In 1998, Seichter and coworkers crystallized the all-inorganic [Al₁₃(OH)₂₄(H₂O)₂₄]¹⁵⁺ (F-Al₁₃, Fig. 1d) as chloride salts through a slow hydrolysis of an aqueous Al³⁺ solution at ambient conditions.³⁷ In 2008, Johnson and coworkers modified the synthetic method for F-Al₁₃ by hydrolyzing an Al³⁺ solution with nitrosobenzene in MeOH, resulting in a high yield.38 However, the high toxicity of nitrosocontaining compounds hindered the large-scale synthesis of F-Al₁₃. To overcome this drawback, in 2011, Keszler and coworkers used Zn metal as a base to hydrolyze Al species, enabling the large-scale preparation of F-Al₁₃.39 Conventional base titration produces a locally high pH environment, facilitating the nucleation of tetrahedral [Al(OH)₄]⁻ species, which condense with six-coordinate Al3+ aqua ions to form a Keggin structure. In contrast, the dissolution of Zn metal gradually increases the pH, offering a direct route to form the F-Al₁₃ clusters with a good yield. In 2013, Cheong, Fang, Keszler, and coworkers electrolytically synthesized F-Al₁₃.40 To increase the pH of Al³⁺-containing solution and produce F-Al₁₃, they utilized the reduction of protons to hydrogen gas in the cathode compartment of a two-compartment electrochemical cell, instead of using a base. They also proposed that F-Al₁₃ forms via an intermediate, $[Al_7(OH)_{12}(H_2O)_{12}]^{9+}$, which represents the planar core of F-Al₁₃, as indicated by Raman spectroscopy and computational studies. The synthesis of F-Al₁₃ can be achieved through both bottom-up and top-down methods. In 2017, Keszler, Hutchison, Johnson, and coworkers synthesized F-Al₁₃ by direct dissolution of aluminum hydroxide in nitric acid.41 They also demonstrated that F-Al₁₃ is applicable as a precursor to

The diversity in cluster size and shape is a notable feature of Al oxo-hydroxide clusters. Cluster downsizing was achieved by inhibiting growth through a decrease in basicity and the use of capping ligands during the hydrolysis of an Al3+ solution. In 2005, Casey and coworkers conducted a long-term (7 years) hydrolysis of an acidic Al³⁺ solution, resulting in the discovery of a smaller Al oxo-hydroxide octamer, $[Al_8(OH)_{14}(H_2O)_{18}]^{10+}$ (Al₈, Fig. 1e).42 The Al₈ cluster exhibits a flat-shaped structure, with the central four [AlO₆] units connected by edge-sharing, while the peripheral four [AlO₆] units are linked through cornersharing. In 2016, Limberg and coworkers trapped Al₈ during the hydrolysis of Al species with the aid of capping ligands (panisylSi(OSiPh₂OH)₃), yielding a trisilanol-capped octameric cluster, $[Al_8(\mu_3-OH)_2(\mu_2-OH)_{10}(THF)_3(p-anisylSi(OSiPh_2O)_3)_4]^{43}$ In 2017, Johnson, Keszler, and coworkers demonstrated a facile synthesis of capping-free Al₈ through the hydrolysis of Al species in a sulfate-rich aqueous solution.44 In 2024, Fang and co-workers conducted the hydrolysis of a *n*-propanolic Al³⁺

prepare near-atomically smooth Al₂O₃ thin films.²⁹

solution with L-valine (L-Val) and pyridine-2,6-dicarboxylic acid (H₂PDA), resulting in the formation of [Al₅O₂(OH)₂(HPDA)₄(L-Val)₄]⁺ (Al₅, Fig. 1f), which features vertex-sharing of two triangles [Al₃O(OH)(HPDA)₂]⁴⁺.⁴⁵ In 2011, Sun and co-workers crystallized a vertex-shared tetrahedral [Al₄(OH)₆(H₂O)₁₂]⁶⁺ (Al₄, Fig. 1g) with [Al(OH₂)₆]³⁺ and Br⁻ as [Al₄(OH)₆(H₂O)₁₂][Al(H₂-O)₆]₂Br₁₂ (Al₄·Al₂Br₁₂) in a cubic $Fd\bar{3}m$ space group.⁴⁶ The tetrahedral Al₄ with T_d symmetry is constructed by the linkage of four distorted [AlO₆] octahedra through vertex-sharing of hydroxyl groups.

Al oxo-hydroxide clusters larger than Al13 have been explored by promoting cluster growth through the hydrolysis of an Al³⁺ solution under relatively harsh conditions-specifically by increasing the basicity of the reaction solution, aging temperature, and reaction times. In 2001, Powell and coworkers performed the hydrolysis of an Al3+ solution with a base (piperazine) and hpdta ligand (H5hpdta = HOCH2[CH2N(CH2- $COOH)_2]_2$, resulting in the formation of $[Al_{15}O_4(OH)_{20}]_2$ $(hpdta)_4]^{3-}$ (Al₁₅, Fig. 1h).⁴⁷ Al₁₅ possesses an inner $\{Al_7(OH)_{12}\}^{9+}$ core, similar to F-Al₁₃, which is encapsulated by four dinuclear {Al₂(hpdta)} units to form Al₁₅. In 2012, Forbes and coworkers refluxed an Al3+ aqueous solution in the presence of 2,6-napthalene disulfonate (2,6-NDS) to obtain [Al26O8(OH)50(H2- O_{20}]¹²⁺ (Al₂₆, Fig. 1i). In Al₂₆, two δ -Al₁₃ clusters are linked *via* vertex-sharing through rotated $[Al_3(\mu_2\text{-OH})_6(H_2O)_3]$ trimer groups. In 2000, $[Al_{30}O_8(OH)_{56}(H_2O)_{26}]^{18+}$ (Al₃₀, Fig. 1j) was synthesized through the thermal hydrolysis of a basic Al³⁺ aqueous solution.33,49 Al NMR studies suggest that Al30 forms when thermal treatment of ε -Al₁₃ produces [AlO₆] units, which then attach to undissociated ε -Al₁₃, promoting isomerization to δ -Al₁₃. Two unstable δ -Al₁₃ monomers stabilize by dimerization with four [AlO₆] units, resulting in the dimeric Al₃₀ structure. In 2010, Bi and coworkers carried out density functional theory (DFT) study and kinetic analysis to address the formation mechanism of Al₃₀.⁵⁰ They proposed a three-step process: (1) isomerization from ε -Al₁₃ to δ -Al₁₃; (2) stabilization of δ -Al₁₃ by Na⁺ to form Na-δ-Al₁₃, followed by replacement of Na⁺ with Al monomers in solution to produce δ -Al₁₄; and (3) reaction of two δ-Al₁₄ with two Al monomers, leading to the formation of Al₃₀. In 2012, Forbes and coworkers reported that Al₃₀ can be crystallized with 2,6-NDS as (Al₂O₈Al₂₈(OH)₅₆(H₂O)₂₆)(2,6-NDS)₈-Cl₂(H₂O)₃₄.48 In 2011, Sun and coworkers conducted the hydrolysis of an Al3+ aqueous solution under hydrothermal conditions to obtain $[Al_{32}O_8(OH)_{60}(H_2O)_{28}(SO_4)_2]^{16+}$ $(Al_{32},$ Fig. 1k). Al₃₂ possesses a structure similar to that of Al₃₀, but with four μ_1 - H_2 O molecules, which exhibit strong acidity in Al_{30} , replaced by two [Al(OH)₂(H₂O)₃(SO₄)]⁻ groups. In 2021, Fang, Zhang, and coworkers synthesized Al₃₂ with a hydrotalcite-like nanoflake structure, $[Al_{32}(benzoate)_{36}(O^iPr)_4(\mu_3-O)_{24}(\mu_4-O)_4]$ (NF-Al₃₂, Fig. 1l), by controlling the hydrolysis of Al³⁺ ions in the presence of π -conjugated carboxylate ligands.⁵²

The size control of ring-shaped Al oxo-hydroxide clusters as well as spherical and elliptical clusters has been achieved. In 2020, Fang, Zhang, and coworkers synthesized ring architectures of Al oxo-hydroxide clusters with general formula $[Al(OH)_x(OR)_y(R'OOCPh)_{3-x-y}]$ (x = 0, y = 2; x = 0.5, y = 1; R = Me, Et, nPr , nBut ; R' = H, F, Cl, NH₂, NO₂, CH₃) by solvothermal

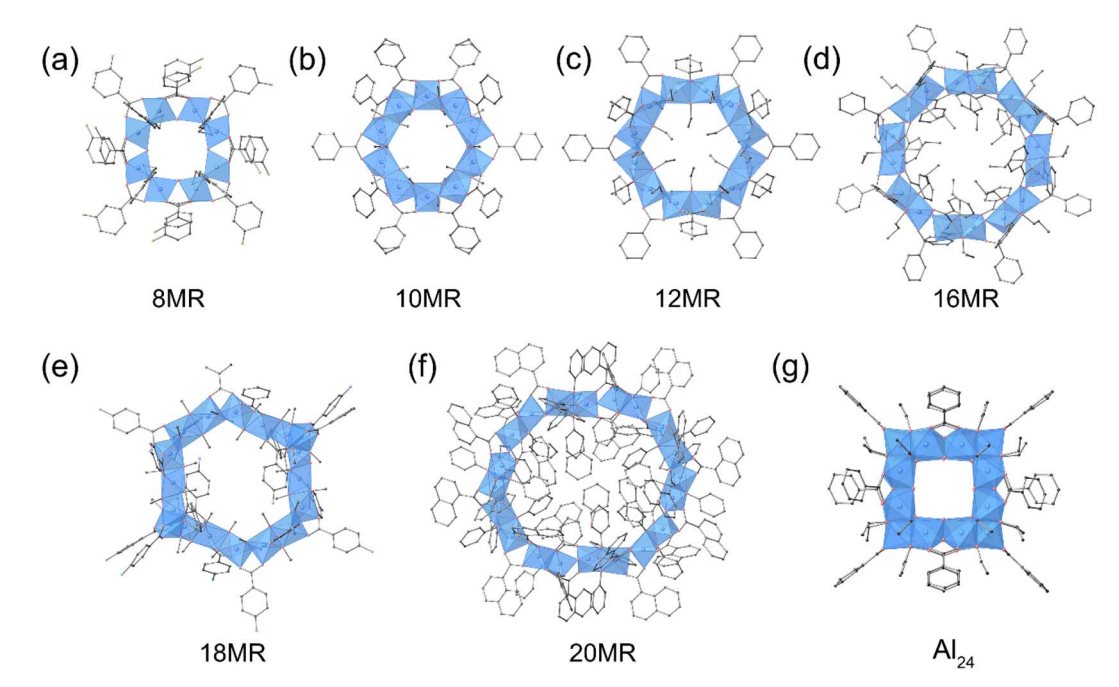


Fig. 2 Molecular structure of (a) $[Al_8(OH)_4(3-fluorobenzoate)_{12}(OBut'')_8]$ (8MR), (b) $[Al_{10}(benzoate)_{10}(OMe)_{20}]$ (10MR), (c) $[Al_{12}(benzoate)_{12}(-OEt)_{24}]$ (12MR), (d) $([Al_{16}(OH)_8(benzoate)_{24}(OPr'')_{16}]$ (16MR), (e) $[Al_{18}(4-aminobenzoate)_{18}(OMe)_{36}]$ (18MR), (f) $[Al_{20}(phenol)_{20}(OH)_{10}(1-naphthalenecarboxylate)_{30}]$ (20MR), and (g) $[Al_{24}(BA)_{12}(EtO)_{24}(OH)_{32}]^{4+}$ (Al₂₄).

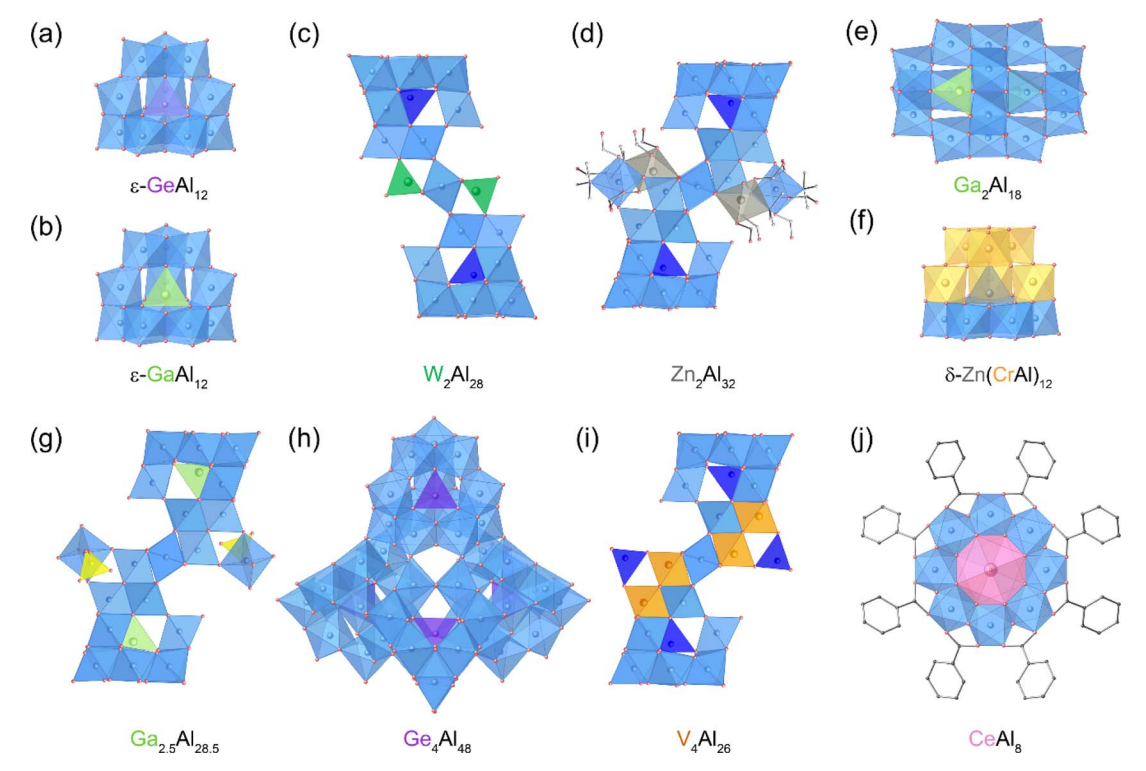
method.⁵³ The proper choice of the type of monohydric alcohols and benzoate derivatives could systematically tune the ring size of clusters from 8-membered ring (8MR, [Al₈(OH)₄(3fluorobenzoate)₁₂(OButⁿ)₈], Fig. 2a) to **10MR** [Al₁₀(benzoate)₁₀(- $OMe)_{20}$, Fig. 2b), 12MR ([Al₁₂(benzoate)₁₂(OEt)₂₄], Fig. 2c), and **16MR** ([Al₁₆(OH)₈(benzoate)₂₄(OPrⁿ)₁₆], Fig. 2d). In 2022, the same group expanded the ring size to 18MR ([Al₁₈(4aminobenzoate)₁₈(OMe)₃₆] Fig. 2e) by introducing hydrophilic amide functional groups,54 and 20MR ([Al20(phenol)20(OH)10(1naphthalenecarboxylate)30], Fig. 2f) through phenol-thermal synthesis.55 In 2022, the same group constructed an Al oxohydroxide cluster with a cage structure, [Al₂₄(benzoate)₁₂(-EtO₂₄(OH)₃₂ $]^{4+}$ (Al₂₄, Fig. 2g), by refluxing an Al³⁺ ethanolic solution with benzoate ligands.56 The Al24 cage features a truncated hexahedron topology and is composed of six octagonal Al₈ faces and eight triangular Al₃ faces, forming an internal cavity with a volume of approximately 320 $Å^3$.

2.2 Metal substituted Al oxo-hydroxide clusters

Since alumina-based solid solutions (*e.g.*, Cr³⁺-doped alumina, ruby) and mixed oxides (*e.g.*, MgAl₂O₄, spinel) exhibit interesting functionalities distinct from those of pure oxides,^{57,58} incorporating other metals into Al oxo-hydroxide clusters would also be a promising approach to explore the compositional and structural diversity, and potential applications. An early work involves the substitution of Ge⁴⁺ ions for the central tetrahedral [AlO₄] in ε-Al₁₃, forming [ε-GeO₄Al₁₂(OH)₂₄(H₂O)₁₂]⁸⁺ (ε-GeAl₁₂, Fig. 3a). ε-GeAl₁₂ was synthesized by Görz, Schönherr, and coworkers in 1983 through the hydrolysis of a mixed aqueous solution containing Al³⁺ and Ge⁴⁺ ions.⁵⁹ In 2001, Casey and

coworkers investigated the molecular structure of ε-GeAl₁₂ using single-crystal X-ray diffraction and solid-state ²⁷Al MAS NMR spectroscopy.60 Their investigations revealed that ε-GeAl₁₂ exhibits an overall point group symmetry of D_{2h} , whereas ε -Al₁₃ shows T_d symmetry. The substitution of Ge^{4+} in the central position induces a tetragonal distortion in ε-GeAl₁₂, characterized by a slight expansion in both axial and equatorial directions. Görz, Schönherr, and coworkers synthesized a Gasubstituted Al cluster with T_d symmetry, [ε-GaO₄Al₁₂(OH)₂₄(H₂-O)₁₂]⁷⁺ (ε-GaAl₁₂, Fig. 3b) through the hydrolysis of a mixed aqueous solution containing Al3+ and Ga3+ ions.61,62 Kydd and coworkers characterized ε-GaAl₁₂ by MAS NMR, IR, and PXRD, highlighting that the central tetrahedral [GaO₄] in ε-GaAl₁₂ was less distorted than [AlO₄] in ε-Al₁₃.63 In 1997, Parker and coworkers demonstrated that the substitution of only Ga³⁺ ions in ε-Al₁₃ proceeded preferentially among Fe³⁺, Zn²⁺, Ga³⁺, In³⁺, Sn²⁺, La³⁺, and Bi³⁺ ions.⁶⁴ More recently, in 2015, Navrotsky and coworkers calculated the formation enthalpies of ε-Al₁₃, ε-GaAl₁₂, and ε-GeAl₁₂ using solution calorimetry and found that stability increase in the order of ε -GeAl₁₂ < ε -GaAl₁₂ < ε -Al₁₃, indicating that changes in element and charge decrease stability.65,66 Importantly, ε-Al₁₃ and its derivatives lie closer in energy to solid-state Al oxides and hydroxides than to aqueous Al monomer ions, suggesting their role as metastable precursors of solid-state materials.

In 2003, Kwon and coworkers extended the transition metal substitution to larger Al_{30} clusters, resulting in W-substituted $[W_2Al_{28}O_{18}(OH)_{48}(H_2O)_{24}]^{12+}$ (W_2Al_{28}) clusters (Fig. 3c).⁶⁷ W_2Al_{28} was produced by reacting Al_{30} with $[H_2W_{12}O_{40}]^{6-}$ as the W source. In W_2Al_{28} , two of the four $[AlO_4]$ units between monomeric Al_{13} of dimeric Al_{30} were replaced with $[WO_4]$. In



structure of (a) $[\epsilon - GeO_4Al_{12}(OH)_{24}(H_2O)_{12}]^{8+}$ $(\epsilon - GeAl_{12})$, (b) $[\epsilon - GaO_4Al_{12}(OH)_{24}(H_2O)_{12}]^{7+}$ 3 Molecular $[W_2Al_{28}O_{18}(OH)_{48}(H_2O)_{24}]^{12+} \ (W_2Al_{28}), \ (d) \ [(Zn(NTA)H_2O)_2(Al(NTA)(OH)_2)_2(Al_{30}O_8(OH)_{60} \ (H_2O)_{20}]^{18+} \ (Zn_2Al_{32}), \ (e) \ [Ga_2Al_{18}O_8(OH)_{36}(H_2O)_{12}]^{8+} \ (U_2Al_{28}O_{18}(OH)_{48}(H_2O)_{24})^{12+} \ (U_2Al_{28}O_{18}(OH)_{48}(OH$ [AlO₆], [AlO₄], and [SO₄] are shown by the light blue, dark blue, and yellow polyhedrons, respectively.

2013, Forbes and coworkers reported Zn-substituted Zn₂Al₃₂ cluster with the formula of [(Zn(NTA)H₂O)₂(Al(NTA)(OH)₂)₂- $(Al_{30}O_8(OH)_{60}(H_2O)_{20}]^{18+}$ (NTA = nitrilotriacetic acid, Fig. 3d).⁶⁸ Zn₂Al₃₂ contains Al₃₂ clusters with two additional [ZnO₆] units chelated by NTA, which are connected to the central part of Al₃₂.

Metal-substitution in Al oxo-hydroxide clusters can lead to the discovery of unprecedented structure motifs. In 2015, Mason, Forbes, and coworkers reported cationic variations on the Wells-Dawson topology, $[Ga_2Al_{18}O_8(OH)_{36}(H_2O)_{12}]^{8+}$ (Ga₂Al₁₈, Fig. 3e), by hydrolyzing a mixed aqueous solution containing Al3+ and Ga3+ ions using a low-temperature hydrothermal method.69 Ga₂Al₁₈ cluster has a metal ratio similar to the typical Wells-Dawson structure $[X_2M_{18}O_{62}]^{n-}$. However, the structural topology of Ga₂Al₁₈ differs from that of anionic Wells-Dawson-type POMs. Ga₂Al₁₈ clusters are composed of a complete ε-Keggin cluster unit (ε-GaAl₁₂) linked to a lacunary fragment, which includes a hexametric unit consisting of one $[Al_3(\mu_2-OH)_6(H_2O)_3]$ trimer and three additional edge-sharing Al(III) octahedra bonded on the exterior edges. In contrast, Wells-Dawson-type POMs are composed of two α-Keggin fragments.

Substitution of multiple types of transition metal ions into Al oxo-hydroxide clusters has been achieved. In 2016, Nyman and coworkers reported the incorporation of Zn²⁺ and Cr³⁺ ions into $\left[\delta\text{-ZnO}_4\text{Al}_{5.1}\text{Cr}_{6.9}(\text{OH})_{24}(\text{H}_2\text{O})_{12}\right]^{6+}$ Zn(CrAl)₁₂, Fig. 3f), where the rotated trimer units are capped

with $[Zn(H_2O)_3]^{2+}$. 70 δ -Zn(CrAl)₁₂ was obtained by evaporating an aqueous solution with high concentrations of Al, Cr, and Zn species. X-ray structure and derived bond valence sums (BVSs) suggest that Zn^{2+} ions are located in the tetrahedral center of δ -Zn(CrAl)₁₂, while Al³⁺/Cr³⁺ ions occupy the octahedral sites with site disordering. The Al/Cr ratios are higher near the rotated trimer units. In 2021, Mason and coworkers demonstrated the substitution of Cr3+ ions in δ-Al13 to synthesize [AlO4Al9.6- $Cr_{2.4}(OH)_{24}(H_2O)_{12}]^{7+}$ (δ -Al_{10.6}Cr_{2.4}).⁷¹ DFT study suggested that Cr³⁺ substitution occurs exclusively at the octahedral positions.

Formation of larger clusters using metal-substituted Albased clusters as building units has been demonstrated. In 2020, Forbes and coworkers synthesized [δ-GaO₄Al₁₂(OH)₂₄- $(H_2O)_{12}$ ⁷⁺ (δ -GaAl₁₂), where the central tetrahedral site was substituted with [GaO₄], by thermal aging of ε-GaAl₁₂.⁷² The reaction of δ-GaAl₁₂ with an aqueous K₂SO₄ solution forms a larger cluster of $[Ga_2O_8Al_{28.5}Ga_{0.5}(OH)_{58}(H_2O)_{27}(SO_4)_2]^{15+}$ $(Ga_{2.5}Al_{28.5}, Fig. 3g)$: the core cluster $Ga_{2.5}Al_{27.5}$, which is isostructural with Al30, is connected with an additional anionic unit ($[Al(OH)_2(H_2O)_3(SO_4)]^-$). X-ray structural analysis indicates that the Ga occupancy in Ga2.5Al28.5 is the highest at the tetrahedral center sites (99.0%) and the second highest at the octahedral sites that bridge the nanocluster halves in the beltway region (26.9%). In 2021, the same group synthesized a giant (ca. 2.4 nm) Ge-substituted cluster, $[Ge_4O_{16}Al_{48}(OH)_{108}(H_2O)_{24}]^{20+}$ (Ge₄Al₄₈, Fig. 3h), by thermally aging ε-GeAl₁₂.⁷³ In Ge₄Al₄₈, four

 ϵ -GeAl₁₂ units are linked *via* twelve μ_2 -OH bridging groups in a $T_{\rm d}$ arrangement. DFT calculations indicated that Ge substitution at the central tetrahedral site of ϵ -GeAl₁₂ is essential for forming the tetrameric Ge₄Al₄₈, as this substitution facilitates the deprotonation of η_1 -H₂O to form symmetric μ_2 -OH bridges, which can then link together to form the tetrameric Ge₄Al₄₈. In 2022, we reported a V-substituted $[V_4Al_{28}O_{20}(OH)_{52}(H_2O)_{22}]^{12+}$ $(V_4Al_{28}, Fig. 3i)$ cluster by reacting δ -Al₁₃ with $[PW_9V_3O_{40}]^{6-}$ as a V⁵⁺ source using a low-temperature hydrothermal method.⁷⁴ V_4Al_{28} contains two δ - VAl_{12} units, which is similar to δ - Al_{13} , but with one [AlO₆] unit of the 60°-rotated [Al₃O₁₃] trimer replaced with a $[VO_6]$ unit. The δ -VAl₁₂ units are bridged by two $[AlO_6]$ and two [VO₆] through corner-sharing and edge-sharing, respectively, to form V₄Al₂₆, which is isostructural with Al₃₀. The two additional [AlO₄] units each link two [VO₆] of V₄Al₂₆ through corner-sharing, resulting in V_4Al_{28} with C_{2h} symmetry.

The incorporation of metal ions into Al oxo-hydroxide clusters has been extended to rare earth ions. In 2023, Fang and coworkers heated a mixture of Al^{3+} ions and lanthanide (Ln) ions with benzoic acid, pyridine, and tetraethylammonium chloride in MeCN at 80 °C, resulting in the formation of $[Al_8Ln(\mu_2\text{-OH})_8(\mu_3\text{-OH})_8(\text{benzoate})_8(H_2O)_2]^{3+}$ (Ln = La³⁺, Ce³⁺, Pr³⁺, and Nd³⁺), **LnAl**₈, Fig. 3j). In **LnAl**₈, Ln ions are situated at the center of the Al_8 ring clusters.

3. Assembly of Al oxo-hydroxide clusters for functional applications

3.1 Adsorption and coagulation

Adsorption and coagulation are fundamental techniques for the removal of targeted substances, and have practical applications in diverse fields, including separation science and environmental chemistry. In particular, adsorption involves the uptake of substances by a solid adsorbent through chemical and/or physical interactions between the substances and the surface of the adsorbent. Coagulation, on the other hand, is a process that occurs during precipitation, wherein additional substances are incorporated into the particles as they form from a solution. In particular, aluminum hydroxides are widely used as adsorbents and in coagulation processes due to the amphoteric character and multiple types of interactions. Adsorption and coagulation processes involve various interactions (Coulombic and van der Waals interactions), bonding mechanisms (hydrogen and covalent bonds), and surface ligand exchanges (OH/X, where X represents halogen ions, etc.). These interactions are facilitated by the cationic nature of aluminum and the presence of labile hydroxide and aqua ligands. Therefore, a promising approach to grant adsorptive properties to Al oxohydroxide cluster-based materials is to increase the surface area and construct a porous structure. A landmark work in this field was reported by Kwon and coworkers in 2000, where they demonstrated that an ionic crystal of ε-Al₁₃ and Anderson-type POM $[Al(OH)_6Mo_6O_{18}]^{3-}$ $(AlMo_6)$, $[\epsilon-AlO_4Al_{12}(OH)_{24}(H_2O)_{12}]$ $[Al(OH)_6Mo_6O_{18}]_2(OH) \cdot 29.5H_2O$ (ϵ -Al₁₃-AlMo₆, Fig. possesses porous 2D channels with dimensions estimated to be $3.1 \times 5.9 \text{ Å}^2$ for the smallest and $6.2 \times 3.9 \text{ Å}^2$ for the widest

cross-sectional areas, showing reversible water adsorption properties. Later, they constructed various porous ionic crystals by changing the combination Al oxo-hydroxide clusters and POMs. 67,82,83

The formation of supramolecular cage crystals is a promising method to build porous structures. In 2021, Fang, Zhang, and coworkers assembled an eight-membered Al₈ ring, [Al₈(4chloropyrazolate)₈(OH)₈(benzoate)₈], through π - π interactions between adjacent Al₈ rings.⁷⁶ As a result, a (Al₈)₆ nanocage (AlOC-27-NC), in which six Al₈ rings occupying the six faces of the cube, was constructed. AlOC-27-NC demonstrates a high iodine (I2) vapor saturation uptake capacity of 503 mg g⁻¹ at 80 °C, attributed to strong $I \cdots \pi$ interactions between molecular I_2 and the phenyl-based linkers of AlOC-27-NC (Fig. 4b). In 2021, the same group demonstrated coordination-driven self-assembly of Al₈ ring, incorporating isonicotinic (INA) linkers, with Cu²⁺ ions to construct $[Al_{12}Cu_5(OH)_6(INA)_{18}(OPr^n)_{12}(H_2O)_2] \cdot 5NO_3^-$ (AlOC-83).84 AlOC-83 exhibits a remarkable capacity for the rapid removal of I2 from cyclohexane solutions, with a considerable loading capacity of 555 mg g⁻¹. In 2022, the same group synthesized an Al24 cluster-based cage structure with benzoate ligands, $[Al_{24}(benzoate)_{12}(EtO)_{24}(OH)_{32}] \cdot (NO_3)_4 \cdot (HOEt)_2 \cdot (H_2O)_2$ (AlMC-1).56 The Brunauer-Emmett-Teller (BET) specific surface area of AlMC-1 was estimated to be 233 m² g⁻¹ by the N₂ sorption isotherm at 77 K. AlMC-1 enables rapid iodine capture from lowconcentration aqueous I₂/KI solutions (down to 4 ppm) with the aid of cooperative $I \cdots \pi$, $C-H \cdots I$, and $OH \cdots I$ interaction within the pores. The adsorption capacity using a 100 000 ppm I₂/KI solution was estimated as 820 mg g⁻¹.

In 2023, Maurin, Senker, Inge, Stock, and coworkers reported a series of Al₂₄ cluster-based porous salts with acetate (CH_3COO^-) ligands, $[Al_{24}(OH)_{56}(CH_3COO)_{12}]X_4$ (CAU-55-X, X = Cl⁻, Br⁻, I⁻, HSO₄⁻, Fig. 4c). 85 The N₂ sorption isotherm of CAU-55-Cl at 77 K suggests a high BET specific surface area of 490 m² g^{-1} . Because of the cationic nature of the Al₂₄ clusters, in particular, CAU-55-HSO₄ effectively adsorbs the anionic dye Alizarin Red S (ARS), with a high adsorption capacity of 239 mg g^{-1} . In 2022, Li and coworkers employed the Al_{24} cage as a building unit for metal-organic framework (MOF).77 Specifically, the Al₂₄ cage, capped with 4-pyrazolecarboxylate (HPyC⁻), was coordinated with Cu^I ions, resulting in the formation of $[Al_{24}(OCH_3)_{24}(OH)_{32}(HPyC)_6][(HPyC)_2Cu_{0.7}\square_{0.3}]_3 \cdot (CH_3COO) \cdot [Al_{24}(OCH_3)_{24}(OH)_{32}(HPyC)_6][(HPyC)_2Cu_{0.7}\square_{0.3}]_3 \cdot (CH_3COO) \cdot [Al_{24}(OCH_3)_{24}(OH)_{32}(HPyC)_6][(HPyC)_2Cu_{0.7}\square_{0.3}]_3 \cdot (CH_3COO) \cdot [Al_{24}(OCH_3)_{24}(OH)_{32}(HPyC)_6][(HPyC)_2Cu_{0.7}\square_{0.3}]_3 \cdot (CH_3COO) \cdot [Al_{24}(OH)_{32}(HPyC)_6][(HPyC)_2Cu_{0.7}\square_{0.3}]_3 \cdot (CH_3COO) \cdot [Al_{24}(HPYC)_2Cu_{0.7}\square_{0.3}]_3 \cdot (CH_3COO) \cdot [Al_{24$ $Cl_{5.1}$ ($\square = Cu^{I}$ vacancy, **FDM-91**). Furthermore, the [Cu(HPyC)₂] complex linker in **FDM-91** is substituted with 1,1'biphenyl-4,4'-dicarboxylate (BPDC), yielding [Al₂₄(OCH₃)₁₂(-OH)₄₄(HPyC)₆(BPDC)₃]·(CH₃COO)·Cl₃ (**FDM-92**, Fig. 4d), which exhibits exceptional water adsorption capacity (0.53 g g⁻¹ at 298 K) among benchmark MOFs.

Not only crystalline materials but also amorphous materials can be utilized as adsorbents. In 2018, we synthesized amorphous high-surface-area aluminium hydroxide-bicarbonates (Al_{13} -HCO₃) by reacting ϵ - Al_{13} with sodium bicarbonate. In 2020, Al_{13} -HCO₃ was applied as adsorbent to remove the anionic dye methyl orange (MO) from water, achieving over 90% MO removal within 10 min (Fig. 4e). This high removal efficiency is attributed to the electrostatic interaction between the anionic

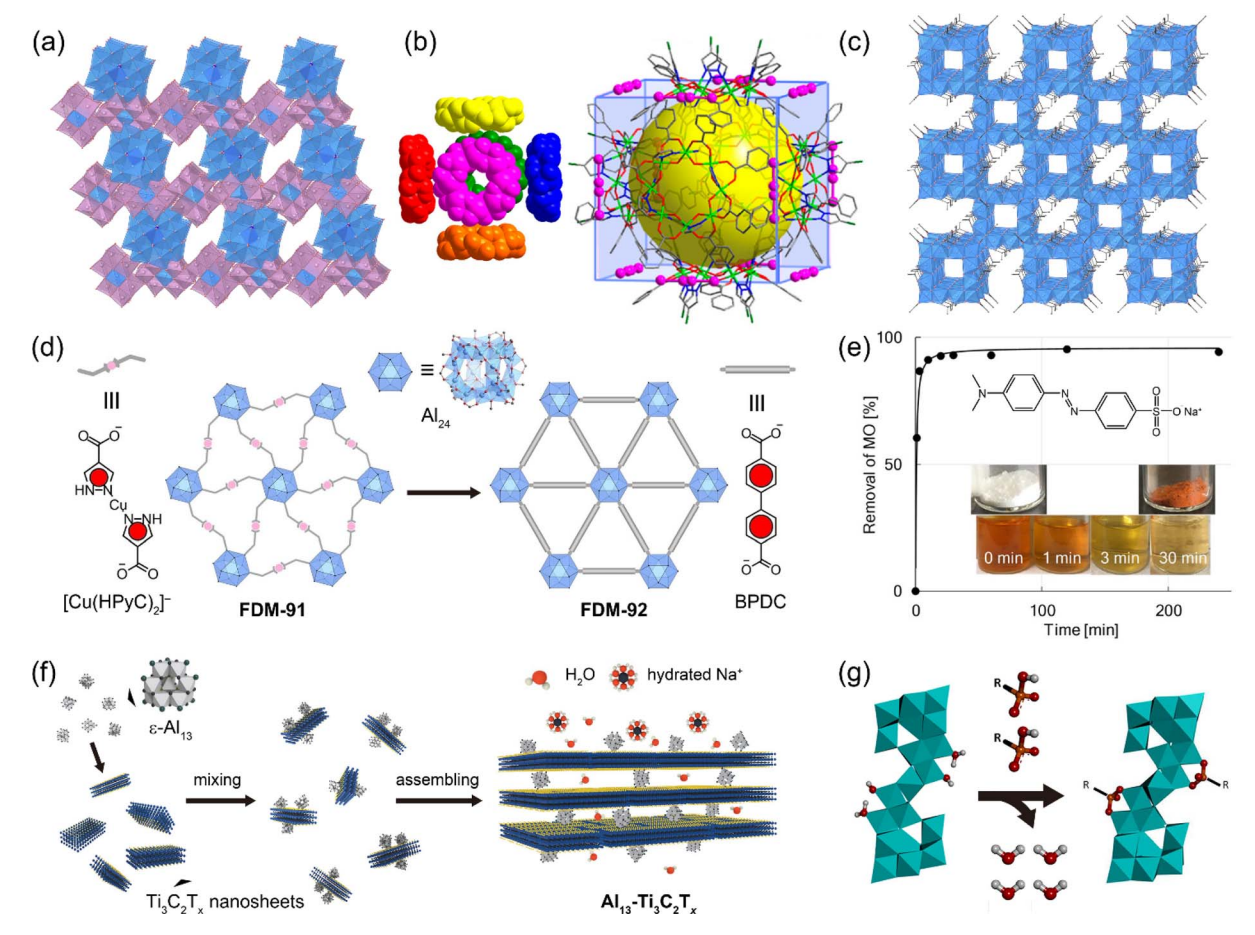


Fig. 4 (a) Crystal structure of $[\epsilon - AlO_4Al_{12}(OH)_{24}(H_2O)_{12}][Al(OH)_6MO_6O_{18}]_2(OH) \cdot 29.5H_2O$ $(\epsilon - Al_{13} - AlMO_6)$. $[AlO_6]$, $[AlO_4]$, and $[MoO_6]$ are shown by the light blue, dark blue, and light magenta polyhedrons, respectively. Water was omitted for clarity. (b) Space-filling representation of the cuboidal (Al₈)₆ nanocage packing in AIOC-26-NC, along with a diagram illustrating the distribution of I₂ molecule around nanocages in AIOC-26-NC (this figure has been reproduced from ref. 76 with permission from the American Chemical Society, copyright 2021). (c) Crystal structure of [Al₂₄(OH)₅₆(CH₃COO)₁₂]Cl₄ (CAU-55-CI), in which chloride was omitted for clarity. (d) Structural transformation from FDM-91 to FDM-92 by linker exchange (this figure has been reproduced from ref. 77 with permission from the Wiley-VCH GmbH, copyright 2023). (e) Time course of removal of MO from water with Al₁₃-HCO₃. Experimental data (closed circles) were fitted with the pseudo-second-order model (black line, this figure has been reproduced from ref. 78 with permission from the American Chemical Society, copyright 2020). (f) Schematic illustration of the fabrication of 2D lamellar Al_{13} - $Ti_3C_2T_x$ (this figure has been reproduced from ref. 79 with permission from the American Chemical Society, copyright 2020). (g) A graphical depiction of the adsorption reaction of t-butylphosphonate (TBP) to Al_{30} to form [(TBP)₂Al₂(μ_4 -O₈)(Al₂₈(μ_2 -OH)₅₆ $(H_2O)_{27}$)¹⁴⁺ (this figure has been reproduced from ref. 80 with permission from the American Chemical Society, copyright 2015).

MO and the coordinatively unsaturated cationic Al₁₃ species, which form under slightly basic synthetic conditions.

Hybridization of Al oxo-hydroxide clusters is also effective in forming porous structures. In 2020, Wang and coworkers fabricated 2D lamellar membranes using ε-Al₁₃ as pillars in 2D $Ti_3C_2T_x$ nanosheets, where T_x represents surface functional groups such as -OH, -F, and =O (Fig. 4f).79 The interlayer spacing of Al₁₃-Ti₃C₂T_x can be precisely modulated with angstrom-level accuracy over a wide range (2.7-11.2 Å) to achieve selective ion sieving. Al₁₃-Ti₃C₂T_r was applied in osmosis desalination processes, demonstrating high NaCl exclusion (99%) with a fast water flux (0.30 L $m^{-2} h^{-1} bar^{-1}$).

Al oxo-hydroxide clusters are also suitable as coagulants in wastewater treatment. In particular, polyaluminum chloride (PACl), obtained by the hydrolysis of aqueous AlCl₃ solution, is a commonly used coagulant that achieves superior removal of dissolved organic carbon (DOC) compared to alum.87 PAC includes three Al species: monomeric Ala, medium polymeric Al_b , and high polymeric Al_c . 88,89 It is generally believed that one of the Al_b and Al_c species corresponds to Al₁₃ and Al₃₀, respectively.90 The charge neutralization capacity of PACl with a high Al₃₀ content (PAC-Al₃₀) is slightly lower than that of PACl with a high Al_{13} content (PAC-Al₁₃) at pH \geq 6.8, whereas it is higher pH $\leq 6.5.^{91}$ The use of Al oxo-hydroxide clusters as coagulants has been explored not only with PACIs that contain a mixture of clusters of various sizes, but also with isolated single-size clusters. In 2015, Forbes, Mason, and coworkers employed Al₃₀ to remove an organo-phosph(on/in)ate, t-butylphosphonate (TBP), from an aqueous solution.80 TBP coordinated in the central beltway region of Al₃₀ and formed a bridging bidentate configuration through ion-pair formation and ligand exchange, resulting in the formation of $[(TBP)_2Al_2(\mu_4-O_8)(Al_{28}(\mu_2-D_8))]$

Perspective

 $OH)_{56}(H_2O)_{22}]^{14+}$ (Fig. 4g). In 2021, Shohel, Forbes, and coworkers demonstrated the removal of humic acid (HA) from Iowa river water by coprecipitating with ε-Al₁₃, ε-GaAl₁₂, or ε-GeAl₁₂.92 The HA removal efficiency increased with decreasing pH, reaching ca. 85% at pH = 5 for all three clusters, due to the presence of labile protons on their surfaces, which enable the neutralization of HA.

3.2 Catalysis

Catalysts mediate various chemical reactions and play a crucial role in chemical production.93 Al oxo-hydroxide clusters possess large numbers of hydroxyl/aqua ligands and have been applied as Brønsted acid catalysts. In 2016, we reacted ε-Al₁₃ with Keggin-type POM $\left[\alpha\text{-CoW}_{12}\text{O}_{40}\right]^{6-}$ (CoW₁₂) to crystallize needle-type crystals of $[\epsilon - Al_{13}O_4(OH)_{24}(H_2O)_{12}][\alpha - CoW_{12}O_{40}](OH) \cdot nH_2O \quad (\epsilon - Al_{13} - CoW_{12} - N)$ possessing nanochannels with an aperture of ca. 6 Å \times 6 Å. 4 \times 6 Å. 4 \times 6 Å. CoW12-N exhibited moderate catalytic activity for the acidcatalyzed pinacol rearrangement at 100 °C for 40 h in toluene (with 31% conversion and 18% yield of pinacolone, Fig. 5a). We found that adding NaCl to the synthetic solution of ε-Al₁₃-CoW₁₂-N produced plate-type crystals of ε -Al₁₃-CoW₁₂-P (Fig. 5b), which is a polymorph of ε-Al₁₃-CoW₁₂-N. ε-Al₁₃-CoW₁₂-P possesses multiple hydrogen bonds between $\epsilon\text{-}Al_{13}$ and CoW_{12} and is structurally stable, featuring one-dimensional channels with an aperture of ca. 12 Å \times 6 Å, which is larger than that of ε -Al₁₃-CoW₁₂-N (ca. 6 Å \times 6 Å). We concluded that the formation of ε -Al₁₃-CoW₁₂-P is attributed to the deshielding of electrostatic interaction between ε-Al₁₃ and CoW₁₂ by Na⁺ and Cl⁻, which slows crystallization and allows the transformation into a more stable polymorph with a larger number of hydrogen bonds. The catalytic activity of ε-Al₁₃-CoW₁₂-P (with 76% conversion and 54% yield of pinacolone) is higher than that of E-Al₁₃-CoW₁₂-N (with 31% conversion and 18% yield of pinacolone) under the same reaction conditions. These results demonstrate that controlling crystal polymorph, which lead to the expansion of channel apertures, improves catalytic activity.

Additionally, we investigated the isomeric effect of Al₁₃ on catalytic activity. In 2021, we crystallized δ-Al₁₃, which is a rotational isomer of ε-Al₁₃, with CoW₁₂ to construct [δ-Al₁₃- $O_4(OH)_{24}(H_2O)_{12}][\alpha - CoW_{12}O_{40}](OH) \cdot nH_2O$ $(\delta-Al_{13}-CoW_{12},$ Fig. $5c)^{67,96}$ δ -Al₁₃-CoW₁₂ effectively catalyzed pinacol rearrangement at 100 °C and 10 h in toluene (with 100% conversion and 75% yield of pinacolone), which is superior to that of ε-Al₁₃-CoW₁₂-N under identical conditions. The enhanced catalytic activity of δ-Al₁₃-CoW₁₂ is attributable to increased Brønsted acidity in δ -Al₁₃. The increased acidity in δ -Al₁₃ can be explained by the shorter average Al-O bond distance in δ-Al₁₃ compared to ε-Al₁₃, as a shorter Al-O distance weakens the O-H bond of the aqua ligand, thereby increasing Brønsted acidity.

Supramolecular cages based on Al oxo-hydroxide clusters have shown promise as heterogeneous catalysts. In 2023, Fang, Zhang, and coworkers reported an intriguing hydrogen bonding assembly from convex-concave $[Al_6Co_3(OH)_4(CAT)_3(HCAT)_9]^{5+}$ $(H_2CATs =$ catechol ligands) into a truncatedhexahedron Archimedean {Al₆Co₃}₈ supramolecular cage, [(Al₆Co₃(OH)₄(CAT)₃(HCAT)₉)₈· $nDMF \cdot 8OAc \cdot 7CAT \cdot 2HCAT \cdot 12O^{i}Pr]^{4+}$ (n = 0-18). The supramolecular cage effectively catalyzed the aldol condensation of acetone and p-nitrobenzaldehyde to yield β-hydroxy ketone at 60 °C and 48 h in DMSO, achieving a 75% yield.

Al oxo-hydroxide clusters can function not only as Brønsted acid catalysts but also as Lewis acid catalysts. In 2022, we crystallized $[V_4Al_{28}O_{20}(OH)_{52}(H_2O)_{22}]^{12+}$ $(V_4Al_{28}, Fig. 3i)$ with $[PW_9V_3O_{40}]^{6-}$ (PW_9V_3) to form $[V_4Al_{28}O_{20}(OH)_{52}(H_2O)_{22}][\alpha PW_9V_3O_{40}]_2 \cdot 55H_2O (V_4Al_{28}-PW_9V_3).^{74} V_4Al_{28}$ possesses exposed [AlO₄] tetrahedra, which are expected to act as Lewis acid sites.

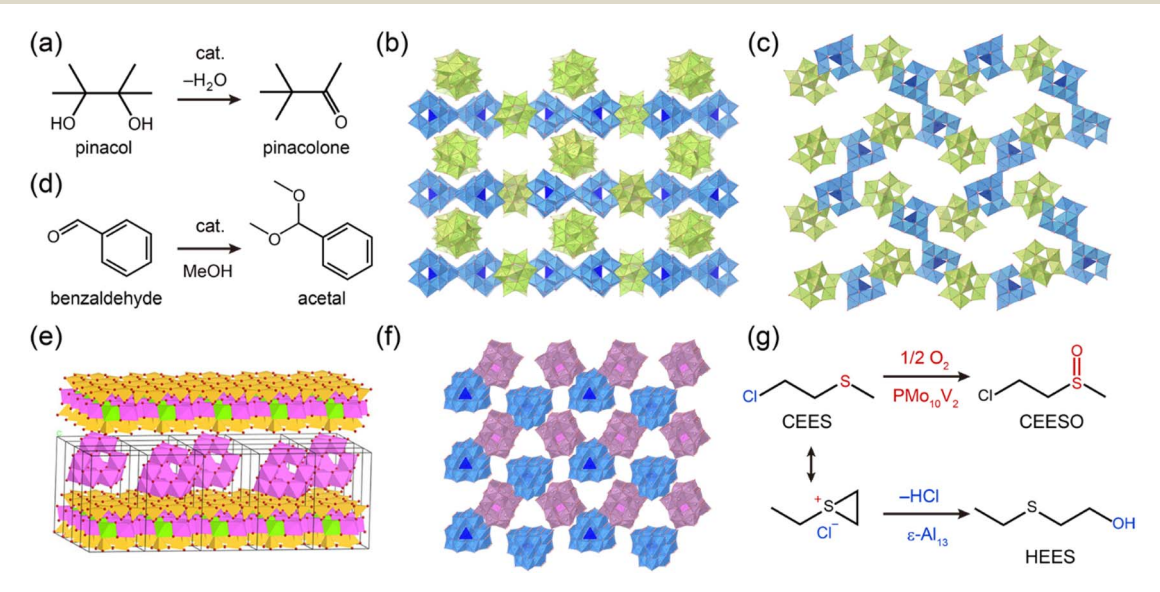


Fig. 5 (a) Acid-catalyzed pinacol rearrangement. Crystal structure of (b) $[\epsilon-Al_{13}O_4(OH)_{24}(H_2O)_{12}][\alpha-CoW_{12}O_{40}](OH)\cdot nH_2O$ $(\epsilon-Al_{13}-CoW_{12}-P)$ and (c) $[\delta-Al_{13}O_4(OH)_{24}(H_2O)_{12}][\alpha-CoW_{12}O_{40}](OH)\cdot nH_2O$ ($\delta-Al_{13}-CoW_{12}$). [AlO₆], [AlO₄], and [CoO₄] are shown by the light blue, dark blue, and light pink polyhedrons, respectively. (d) Acetalization of benzaldehyde with methanol. (e) Arrangement models of &-Al₁₃ in the interlayer region of montmorillonite (this figure has been reproduced from ref. 95 with permission from the American Chemical Society, copyright 2019). (f) Crystal structure of $[\epsilon-Al_{13}O_4(OH)_{24}(H_2O)_{12}][\alpha-PMo_{10}V_2O_{40}](OH)_2 \cdot 20H_2O$ ($\epsilon-Al_{13}-PMo_{10}V_2$). $[AlO_6]$, $[AlO_4]$, $[PO_4]$ and $[MoO_6]$ are shown by the light blue, dark blue, dark pink and light magenta polyhedrons, respectively. (g) Proposed dual-mechanism degradation of CEES by ε-Al₁₃-PMo₁₀V₂.

The catalytic activity of V_4Al_{28} - PW_9V_3 was investigated by acetalization of benzaldehyde with methanol to produce benzaldehyde dimethyl acetal at 70 °C after 2 h (Fig. 5d). The catalytic activity of V_4Al_{28} - PW_9V_3 (with 53% yield) is higher than that of δ - Al_{13} - CoW_{12} (with 41% yield), $[\delta$ - $Al_{13}O_4(OH)_{24}(H_2O)_{12}][PW_9V_3-O_{40}](OH)\cdot 24H_2O$ (δ - Al_{13} - PW_9V_3 , with 40% yield), and ϵ - Al_{13} - CoW_{12} -P (with 41% yield), which do not have the exposed $[AlO_4]$ sites. These observations highlight that the Lewis acid sites of V_4Al_{28} - PW_9V_3 play a critical role in the acetalization reaction.

Chemical Science

Transition metal substituted Al oxo-hydroxide clusters show potential also as electrocatalysts. In 2023, Liu and coworkers reported $[Co_4Al_{12}O_8(OH)_{10}(TBC[4])_4(DMF)_8Cl_2]$ (TBC[4] = tbutylcalix[4]arene) (Co₄Al₁₂) with catalytically active surfaceexposed Co2+ sites.98 The deposition of Co4Al12 on carbon nanotubes (CNTs) forms Co₄Al₁₂/CNT. Co₄Al₁₂/CNT exhibits outstanding electrocatalytic performance for the oxygen evolution reaction (OER), requiring remarkably lower overpotentials in comparison to metal oxide catalysts such as IrO2/CNTs and Co₂O₃/CNTs. Specifically, the overpotential to achieve current density of 10, 50, 100 mA cm⁻² for Co₄Al₁₂/CNT are 320, 414, and 505 mV, respectively, while the corresponding overpotentials for IrO₂/CNTs are 373, 510, and 622 mV, respectively. The superior catalysis of Co₄Al₁₂/CNT is attributable to a binding interaction between the exposed Co sites and OH-, which facilitates the oxidative cleavage of O-H bonds.

Cationic Al oxo-hydroxide clusters can be used to anchor catalytically active anionic species to enhance the activity of the resulting solid catalyst. In 2010, Cabello and coworkers employed $[\epsilon\text{-AlO}_4\text{Al}_{12}(\text{OH})_{24}(\text{H}_2\text{O})_{12}][\text{Al}(\text{OH})_6\text{Mo}_6\text{O}_{18}]_2(\text{OH})$.

29.5H₂O (ε-Al₁₃-AlMo₆, Fig. 4a),⁸¹ where catalytically active AlMo₆ is anchored with ε-Al₁₃ as an oxidation catalyst. 99 ε-Al₁₃-AlMo6 showed excellent catalytic performance in two aromatic sulfide oxidation reactions: the conversion of diphenylsulfide (DPS) to diphenylsulfone in the presence of H₂O₂ (with 100% conversion and selectivity 96% in MeCN at 80 °C for 70 min) and the oxidation of dibenzothiophene (DBT) to dibenzothiophenone using t-BuOOH (with 22.5% conversion in decane at 75 °C for 3 h). In 2019, Zhu, Xi and coworkers utilized ε-Al₁₃ and Al₃₀ as inorganic pillars in montmorillonite (Mt, Fig. 5e). 95,100 The intercalation of ϵ -Al $_{13}$ or Al $_{30}$ into the interlayer region of Mt increases acidity, thereby facilitating the sorption and oxidation of toluene. In 2020, Luo and coworkers hybridized Keggin-type Al₁₃ with redox-active V₂O₅ nanosheets to prepare an Al₁₃-V₂O₅ nanohybrid.101 While pristine V2O5 nanosheets experience agglomeration due to layer stacking, the incorporation of Al₁₃ into the V2O5 nanosheets increases the stacking space and forms porous structures. The porous Al₁₃-V₂O₅ effectively catalyzed the oxidation of benzyl alcohol to benzaldehyde in acetonitrile at 100 °C, 1 atm O2. In 2022, Zhang, Zhong, and coworkers crystalized ε-Al₁₃ with photosensitive meso-tetra(4carboxyphenyl)porphyrin (TCPP⁴⁻) as (TCPP)[ε-Al₁₃O₄(OH)₂₄(- $H_2O)_{12}]_2(OH)_{10} \cdot 18H_2O (Al_{13}-TCPP)^{102} Al_{13}-TCPP$ was applied for the photocatalytic degradation of mustard gas simulant, 2chloroethyl ethyl sulfide (CEES). The degradation rate of CEES for Al₁₃-TCPP in methanol was 96.2% after 3 h, which is higher than that of H_4TCPP (54.7%). All these results indicate that ε -Al₁₃ serves as a favourable anchor for advancing catalytic reactions.

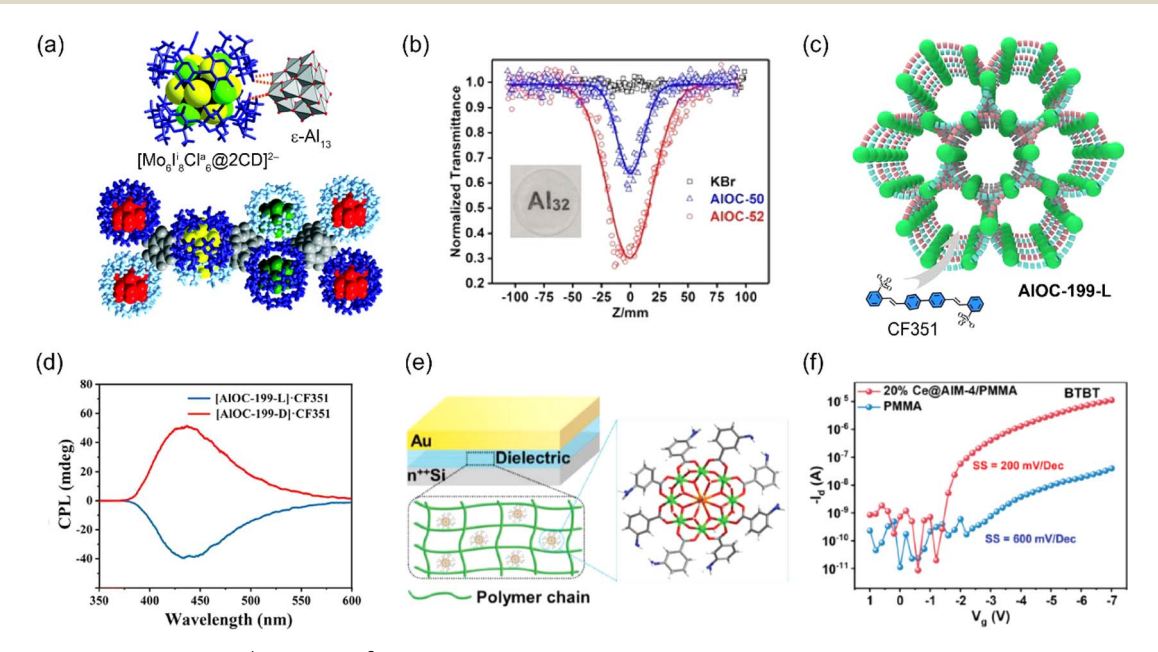


Fig. 6 (a) Interaction between $[Mo_6]^{i}_8 Cl_6^a$ and ε-Al₁₃ and the packing structure of Al₁₃-Mo₆ (this figure has been reproduced from ref. 104 with permission from the Royal Society of Chemistry, copyright 2020). (b) Open-aperture Z-scan results at 532 nm for KBr, AlOC-50, and AlOC-52 (this figure has been reproduced from ref. 52 with permission from the Wiley-VCH GmbH, copyright 2021). (c) Schematic diagram illustrating the doping of fluorescent dye molecules (CF351) in chiral supramolecular structures (AlOC-199-L). (d) Circularly polarized luminescence (CPL)spectra of AlOC-199-L/R·CF351 (this figure has been reproduced from ref. 45 with permission from the American Chemical Society, copyright 2024). (e) Schematic illustration of the capacitor with Ce@AlM-4 doped polymer dielectrics. (f) Transfer curves of the transistor with PMMA and 20% Ce@AlM-4/PMMA dielectrics (this figure has been reproduced from ref. 105 with permission from the Wiley-VCH GmbH, copyright 2023).

Perspective **Chemical Science**

The integration of catalytically active sites from cationic Al oxo-hydroxide clusters and anionic species offers promising potential for the design of solid catalyst. In 2020, Zhang and coworkers reacted ϵ -Al₁₃ with $\left[\alpha$ -PMo₁₀V₂O₄₀ $\right]^{5-}$ (PMo₁₀V₂) to obtain $[\epsilon - Al_{13}O_4(OH)_{24}(H_2O)_{12}][\alpha - PMO_{10}V_2O_{40}](OH)_2 \cdot 20H_2O$ (ϵ - Al_{13} -PMo₁₀V₂, Fig. 5f). ¹⁰³ ε -Al₁₃-PMo₁₀V₂ acts as a dualfunctional catalyst for the degradation of CEES; ε-Al₁₃ hydrolyzes CEES to 2-hydroxyethyl ethyl sulfide (HEES) and PMo₁₀V₂ oxidizes CEES to 2-chloroethyl ethyl sulfoxide (CEESO, Fig. 4g). Thus, ε-Al₁₃-PMo₁₀V₂ exhibits excellent performance for the degradation of CEES with 96.4% conversion in petroleum ether solution at ambient conditions, compared to 47.2% and 21.6% conversion catalyzed by pristine ε -Al₁₃ and PMo₁₀V₂, respectively.

3.3 Other applications

Al oxo-hydroxide clusters have been utilized as components in optical materials, where they modulate the arrangement of luminescent organic molecules and inorganic clusters. In 2020, Falaise, Cordier, and coworkers employed ε-Al₁₃ as a host matrix for luminescent materials.104 Luminescent molybdenum clusters, $[Mo_6I_8^iCl_6^a]^{2-}$, encapsulated in γ -cyclodextrin (CD), were integrated with ε -Al₁₃ to construct {Al₁₃}{[Mo₆Iⁱ₈Cl₆^a]@2CD} Cl₅·60H₂O (Al₁₃-Mo₆, Fig. 6a). The structural void of Al₁₃-Mo₆ was 41%, and its quantum yield of luminescence in the red-near infrared region was 28%. In 2023, Li, Wang, and coworkers synthesized an 8-membered ring cluster, [Al₈(OH)₈(NA)₁₆] (HNA = nicotinic acid), using HNA as a phosphor ligand, and demonstrated its dual luminescence properties, exhibiting fluorescence and room-temperature phosphorescence (RTP).106 Besides, its photoluminescence was effectively regulated by the introduction of CdX_2 ($X = Cl^-$, Br^- , I^-) units.

Al oxo-hydroxide clusters caped with π -conjugated group can serve as third-order nonlinear optical (NLO) materials, with potential applications in photonic technologies, including optical limiting (OL) for eye protection and radiation detectors and sensors. In 2021, Fang, Zhang, and coworkers employed Al₃₂ nanoflake featuring abundant π -conjugated carboxylates, specifically $[Al_{32}(benzoate)_{36}(O^{i}Pr)_{4}(\mu_{3}-O)_{24}(\mu_{4}-O)_{4}]$ (AlOC-50, Fig. 1l) and $[Al_{32}(2-furancarboxylate)_{36}(O^{i}Pr)_{4}(\mu_{3}-O)_{24}(\mu_{4}-O)_{4}]$. 2CH₃CN (AlOC-52), as third-order NLO materials.⁵² The nonlinear absorption coefficient (β) values, estimated by Z-scan curves, were $1.182 \times 10^{-8} \text{ m W}^{-1}$ and $4.384 \times 10^{-8} \text{ m W}$ for AlOC-50 and AlOC-52, respectively (Fig. 6b). These values are superior to those of reported transition metal or rare-earth metal cluster-based materials. In 2022, the same groups studied the third-order NLO properties of ring-shaped Al oxohydroxide clusters with varying sizes and capping linkers.^{54,55} As a result, they found that [Al₂₀(phenol)₂₀(OH)₁₀(pyrenecarboxylate)30]-6phenol (AlOC-76) exhibits the best performance ($\beta = 7.18 \times 10^{-10} \text{ m W}^{-1}$) due to the strongest and diverse π - π interactions. In 2024, the same group reported the crystal-to-glass formation of a ring-shaped Al oxo-hydroxide cluster, [tetramethylammonium] \subset {Cl@[Al₈(phenol)₈(OH)₄(2 $naphthalenecarboxylate)_{12}$ $] \cdot 2phenol \cdot 2DMF$ (Aloc-77TMACl).107 The glassy state of AlOC-77-TMAC exhibited NLO properties similar to those of the crystalline state.

Al oxo-hydroxide clusters possess significant potential for use in low-cost circularly polarized luminescence (CPL) materials. In 2024, Fang and coworkers synthesized a homochiral Al oxo-hydroxide cluster, $[Al_5O_2(OH)_2(HPDA)_4(L-Val)_4] \cdot O^n Pr (Aloc-$ **199-L**· O^n Pr, Fig. 1f), using pyridine-2,6-dicarboxylic acid (H₂PDA) and the chiral L-valine (L-Val) ligand. 45 AlOC-199- $L \cdot O^n$ Pr features a hexagonal one-dimensional channel, in which the OⁿPr⁻ ions were exchanged with an anionic fluores-4,4'-bis(2-sulfostyryl)biphenyl (CF351²⁻), molecule, yielding AlOC-199-L·CF351 (Fig. 6c). AlOC-199-L·CF351 demonstrated significant CPL performance (Fig. 6d), with an absolute luminescence dissymmetry factor (g_{lum}) of up to the order of 10⁻³, which is comparable to several noble metals. 108,109

Recent efforts have focused on using Al oxo-hydroxide clusters as components in electronic devices, specifically field-effect transistors (FETs). In 2023, Fang, Huang, and coworkers incorporated $[Al_8Ce(\mu_2\text{-OH})_8(\mu_3\text{-OH})_8(BA\text{-mNH}_2)_8(H_2O)_2] \cdot 3NO_3$ (Ce@AlM-4), which features a central Ce(III) core connected to eight Al atoms through sixteen bridging hydroxyls and eight 3aminobenzoate (BA-mNH2) ligands, into the polymer-based dielectric layer of FETs (Fig. 6e).105 The capacitance of polymethyl methacrylate (PMMA) films increased 2.9 times after doping with 20% Ce@AlM-4, resulting in a relative permittivity (k) of 9.4 at 20 Hz (Fig. 6f). Furthermore, leakage current and dielectric loss were suppressed, while the dielectric breakdown strength was enhanced. As a result, the on/off ratio of FET-Ce@AlM-4/PMMA (1.3×10^6) is approximately three orders of magnitude higher than that of FET-PMMA (2.7×10^3) . The charge-carrier mobility (µ) of FET-Ce@AlM-4/PMMA reached to $2.45 \text{ cm}^2 \text{ V}^{-1} \text{ s}^{-1}$, which is approximately 50 times higher than that of FET-PMMA.

Summary and outlook

In this perspective, we discussed the syntheses, molecular structures, and functional applications of Al oxo-hydroxide clusters. These clusters are formed through the hydrolysis of Al³⁺-containing solutions, with their diversity in sizes and shapes controlled by adjusting the basicity and utilizing capping ligands. Metal substitution further enhances the compositional and structural diversity. Al oxo-hydroxide clusters have been assembled as ionic crystals, amorphous solids, and hybrid materials, demonstrating functional applications in adsorption and heterogeneous catalysis. They exhibit unique functionalities distinct from those of their anionic counterparts (i.e., POMs) or bulk Al oxides/hydroxides.

We present future outlooks for Al oxo-hydroxide cluster research, focusing on (i) molecular design, (ii) synthetic methods, and (iii) functional applications. For (i) molecular design, developing Al oxo-hydroxide clusters that incorporate a wide range of lanthanide ions, such as Tb³⁺ and Dy³⁺, holds promise for applications in single-molecule magnets (SMMs)110 and single-molecule electrets (SMEs).111 The utilization of these clusters to construct mechanically interlocked molecular architectures, such as catenanes and rotaxanes, presents a key

challenge. 112,113 In terms of (ii) synthetic methods, scalable and environmentally friendly techniques, such as mechanochem-

ical synthesis, are crucial for practical applications. This approach, which involves mechanically activating solid reactants with minimal solvent, offers advantages such as reduced reaction times, increased scalability, and lower costs and environmental impact.114,115 Moreover, it can leverage the high reactivity and structural flexibility of Al oxo-hydroxide clusters. Regarding (iii) functional applications, enhancing adsorption and catalytic properties, as well as exploring other potential applications, is particularly important. Hybridizing Al oxohydroxide clusters with MOFs is expected to increase the overall surface area and adsorption capacity, as observed in POM/ MOF composites. 116,117 Aluminum oxides have been used to anchor metal atoms in single-atom metal catalysts, 118 and the use of Al oxo-hydroxide cluster-based solids is anticipated to fine-tune the local environment of the metal site, thereby enhancing the corresponding reaction activity. Al oxo-hydroxide clusters are characterized by a significant abundance of protons, originating from hydroxyl and aqua groups. These clusters are expected to demonstrate outstanding proton conductivity, similar to the high proton conductivity observed in cationic bismuth oxide clusters.119 It is expected that Al oxohydroxide clusters, as proton donors, can be assembled with anionic proton acceptors to form polar crystals and exhibit ferroelectricity in inorganic molecular crystals. 120 We anticipate that advances in Al oxo-hydroxide clusters will contribute to both fundamental science and practical applications in the future.

Data availability

Chemical Science

The data for this article are available from each literature cited in the reference section. The molecular and crystal structures depicted in Fig. 1-5 are drawn by us using the crystallographic information files (CIFs).

Author contributions

The manuscript was written through the contributions of all authors.

Conflicts of interest

There are no conflicts to declare.

Acknowledgements

This work was supported by grants-in-aid for scientific research (JP24H02211, 24H00463, 23K13759, 23K20034, 23H04613, 23K13759, 22H04914) from MEXT of Japan. Our collaborators inside and outside of Japan, and former and current students of Uchida group are acknowledged for their great contribution to this research.

Notes and references

- 1 M. Nyman, Coord. Chem. Rev., 2017, 352, 461-472.
- 2 D. Yang, M. Babucci, W. H. Casey and B. C. Gates, ACS Cent. Sci., 2020, 6, 1523-1533.
- 3 J. F. Keggin, Nature, 1933, 131, 908-909.
- 4 M. Nyman and P. C. Burns, Chem. Soc. Rev., 2012, 41, 7354-
- 5 Y. F. Song and R. Tsunashima, Chem. Soc. Rev., 2012, 41,
- 6 L. Vilà-Nadal and L. Cronin, Nat. Rev. Mater., 2017, 2, 17054.
- 7 N. I. Gumerova and A. Rompel, Chem. Soc. Rev., 2020, 49,
- 8 N. Ogiwara, T. Iwano, T. Ito and S. Uchida, Coord. Chem. Rev., 2022, 462, 214524.
- 9 W. H. Casey, Chem. Rev., 2006, 106, 1-16.
- 10 Z. L. Mensinger, W. Wang, D. A. Keszler and D. W. Johnson, Chem. Soc. Rev., 2012, 41, 1019-1030.
- 11 Y. Watanabe, K. Hyeon-Deuk, T. Yamamoto, M. Yabuuchi, O. M. Karakulina, Y. Noda, T. Kurihara, I.-Y. Chang, M. Higashi, O. Tomita, C. Tassel, D. Kato, J. Xia, T. Goto, C. M. Brown, Y. Shimoyama, N. Ogiwara, J. Hadermann, A. M. Abakumov, S. Uchida, R. Abe and H. Kageyama, Sci. Adv., 2022, 8, eabm5379.
- 12 K. H. Whitmire and K. Wall, Coord. Chem. Rev., 2023, 488, 215072.
- 13 W. H. Fang, Y. L. Xie, S. T. Wang, Y. J. Liu and J. Zhang, Acc. Chem. Res., 2024, 57, 1458-1466.
- 14 L. M. Cui, W. H. Fang and J. Zhang, Chin. Chem. Lett., 2024, 110386, DOI: 10.1016/j.cclet.2024.110386.
- 15 Y. Zhang, F. de Azambuja and T. N. Parac-Vogt, Coord. Chem. Rev., 2021, 438, 213886.
- 16 D. Van den Eynden, R. Pokratath and J. De Roo, Chem. Rev., 2022, 122, 10538-10572.
- 17 O. Sadeghi, L. N. Zakharov and M. Nyman, Science, 2015, 347, 1359-1362.
- 18 N. P. Martin, C. Volkringer, N. Henry, X. Trivelli, G. Stoclet, A. Ikeda-Ohno and T. Loiseau, Chem. Sci., 2018, 9, 5021-5032.
- 19 H. G. Dill, Earth-Sci. Rev., 2001, 53, 35-93.
- 20 N. D. Priest, J. Environ. Monit., 2004, 6, 375-403.
- 21 H. Pines and W. O. Haag, J. Am. Chem. Soc., 1960, 82, 2471-2483.
- 22 H. Kathyayini, I. Willems, A. Fonseca, J. B. Nagy and N. Nagaraju, Catal. Commun., 2006, 7, 140-147.
- 23 B. N. S. Al-dhawi, S. R. M. Kutty, L. Baloo, A. M. Alawag, N. M. Y. Almahbashi, G. M. A. Naji, Y. A. A. Alsaeedi, F. A. H. Al-Towayti and A. H. Jagaba, Case Stud. Chem. Environ. Eng., 2023, 7, 100350.
- 24 D. Hunter and D. S. Ross, Science, 1991, 251, 1056-1058.
- 25 R. W. Gensemer and R. C. Playle, Crit. Rev. Environ. Sci. Technol., 1999, 29, 315-450.
- 26 G. Furrer, B. L. Phillips, K.-U. Ulrich, R. Pöthig and W. H. Casey, Science, 2002, 297, 2245-2247.
- 27 Y. Sakhawoth, J. Dupire, F. Leonforte, M. Chardon, F. Monti, P. Tabeling, B. Cabane, R. Botet and J. B. Galey, Sci. Rep., 2021, 11, 6376.

28 L. Liu, S. Lu, G. An, B. Yang, X. Zhao, D. Wu, H. He and D. Wang, *Coord. Chem. Rev.*, 2022, 473, 214807.

Perspective

- 29 C. K. Perkins, R. H. Mansergh, J. C. Ramos, C. E. Nanayakkara, D.-H. Park, S. Goberna-Ferrón, L. B. Fullmer, J. T. Arens, M. T. Gutierrez-Higgins, Y. R. Jones, J. I. Lopez, T. M. Rowe, D. M. Whitehurst, M. Nyman, Y. J. Chabal and D. A. Keszler, *Opt. Mater. Express*, 2017, 7, 273–280.
- 30 G. Johansson, G. Lundgren, L. G. Sillén and R. Söderquist, *Acta Chem. Scand.*, 1960, 14, 769–771.
- 31 G. Johansson, Acta Chem. Scand., 1960, 14, 771-773.
- 32 G. Fu, L. F. Nazar and A. D. Bain, *Chem. Mater.*, 1991, 3, 602–610.
- 33 J. Rowsell and L. F. Nazar, *J. Am. Chem. Soc.*, 2000, **122**, 3777–3778.
- 34 S. E. Smart, J. Vaughn, I. Pappas and L. Pan, *Chem. Commun.*, 2013, **49**, 11352–11354.
- 35 A. F. Oliveri, C. A. Colla, C. K. Perkins, N. Akhavantabib, J. R. Callahan, C. D. Pilgrim, S. E. Smart, P. H. Cheong, L. Pan and W. H. Casey, *Chem. Eur. J.*, 2016, 22, 18682– 18685.
- 36 S. L. Heath, P. A. Jordan, I. D. Johnson, G. R. Moore, A. K. Powell and M. Helliwell, *J. Inorg. Biochem.*, 1995, 59, 785–794.
- 37 W. Seichter, H.-J. Mögel, P. Brand and D. Salah, Eur. J. Inorg. Chem., 1998, 1998, 795–797.
- 38 J. T. Gatlin, Z. L. Mensinger, L. N. Zakharov, D. MacInnes and D. W. Johnson, *Inorg. Chem.*, 2008, **47**, 1267–1269.
- 39 W. Wang, K. M. Wentz, S. E. Hayes, D. W. Johnson and D. A. Keszler, *Inorg. Chem.*, 2011, 50, 4683–4685.
- 40 W. Wang, W. Liu, I. Y. Chang, L. A. Wills, L. N. Zakharov, S. W. Boettcher, P. H. Cheong, C. Fang and D. A. Keszler, *Proc. Natl. Acad. Sci. U. S. A.*, 2013, 110, 18397–18401.
- 41 B. L. Fulton, C. K. Perkins, R. H. Mansergh, M. A. Jenkins, V. Gouliouk, M. N. Jackson, J. C. Ramos, N. M. Rogovoy, M. T. Gutierrez-Higgins, S. W. Boettcher, J. F. Conley, D. A. Keszler, J. E. Hutchison and D. W. Johnson, *Chem. Mater.*, 2017, 29, 7760–7765.
- 42 W. H. Casey, M. M. Olmstead and B. L. Phillips, *Inorg. Chem.*, 2005, 44, 4888–4890.
- 43 K. S. Lokare, N. Frank, B. Braun-Cula, I. Goikoetxea, J. Sauer and C. Limberg, *Angew. Chem., Int. Ed.*, 2016, 55, 12325–12329.
- 44 C. K. Perkins, E. S. Eitrheim, B. L. Fulton, L. B. Fullmer, C. A. Colla, D. H. Park, A. F. Oliveri, J. E. Hutchison, M. Nyman, W. H. Casey, T. Z. Forbes, D. W. Johnson and D. A. Keszler, *Angew. Chem., Int. Ed.*, 2017, 56, 10161–10164.
- 45 R.-Q. Chen, S.-T. Wang, Y.-J. Liu, J. Zhang and W.-H. Fang, *J. Am. Chem. Soc.*, 2024, **146**, 7524–7532.
- 46 Z. Sun, H. Wang, H. Feng, Y. Zhang and S. Du, *Inorg. Chem.*, 2011, **50**, 9238–9242.
- 47 W. Schmitt, E. Baissa, A. Mandel, C. E. Anson and A. K. Powell, *Angew. Chem., Int. Ed.*, 2001, **40**, 3577–3581.
- 48 S. Abeysinghe, D. K. Unruh and T. Z. Forbes, *Cryst. Growth Des.*, 2012, **12**, 2044–2051.
- 49 L. Allouche, C. Gérardin, T. Loiseau, G. Férey and F. Taulelle, *Angew. Chem., Int. Ed.*, 2000, **39**, 511–514.

- 50 W. Yang, Z. Qian, B. Lu, J. Zhang and S. Bi, *Geochim. Cosmochim. Acta*, 2010, 74, 1220–1229.
- 51 Z. Sun, H. Wang, H. Tong and S. Sun, *Inorg. Chem.*, 2011, **50**, 559–564.
- 52 Y. J. Liu, Q. H. Li, D. J. Li, X. Z. Zhang, W. H. Fang and J. Zhang, *Angew. Chem.*, *Int. Ed.*, 2021, **60**, 4849–4854.
- 53 L. Geng, C. H. Liu, S. T. Wang, W. H. Fang and J. Zhang, *Angew. Chem., Int. Ed.*, 2020, **59**, 16735–16740.
- 54 Y. Li, C. Zheng, S. T. Wang, Y. J. Liu, W. H. Fang and J. Zhang, *Angew. Chem., Int. Ed.*, 2022, **61**, e202116563.
- 55 S. T. Wang, Y. J. Liu, C. C. Feng, W. H. Fang and J. Zhang, *Aggregate*, 2022, **4**, e264.
- 56 Y. J. Liu, Y. F. Sun, S. H. Shen, S. T. Wang, Z. H. Liu, W. H. Fang, D. S. Wright and J. Zhang, *Nat. Commun.*, 2022, 13, 6632.
- 57 I. Ganesh, Int. Mater. Rev., 2013, 58, 63-112.
- 58 K. Drdlikova, R. Klement, D. Drdlik, D. Galusek and K. Maca, *J. Eur. Ceram. Soc.*, 2020, **40**, 2573–2580.
- 59 S. Schönherr and H. Görz, *Z. Anorg. Allg. Chem.*, 1983, **503**, 37–42.
- 60 A. P. Lee, B. L. Phillips, M. M. Olmstead and W. H. Casey, *Inorg. Chem.*, 2001, 40, 4485–4487.
- 61 B. Thomas, H. Görz and S. Schönherr, *Z. Chem.*, 1987, 27, 183.
- 62 H. Görz, S. Schönherr and F. Pertlik, *Monatsh. Chem.*, 1991, 122, 759–764.
- 63 S. M. Bradley, R. A. Kydd and C. A. Fyfe, *Inorg. Chem.*, 1992, 31, 1181–1185.
- 64 W. O. N. Parker Jr, R. Millini and I. Kiricsi, *Inorg. Chem.*, 1997, **36**, 571–575.
- 65 C. R. Armstrong, W. H. Casey and A. Navrotsky, *Proc. Natl. Acad. Sci. U. S. A.*, 2011, **108**, 14775–14779.
- 66 D. Reusser, W. H. Casey and A. Navrotsky, *Angew. Chem.*, Int. Ed., 2015, 54, 9253–9256.
- 67 J. H. Son, Y.-U. Kwon and O. H. Han, *Inorg. Chem.*, 2003, 42, 4153–4159.
- 68 S. Abeysinghe, D. K. Unruh and T. Z. Forbes, *Inorg. Chem.*, 2013, 52, 5991–5999.
- 69 M. Fairley, K. W. Corum, A. Johns, D. K. Unruh, M. Basile, J. de Groot, S. E. Mason and T. Z. Forbes, *Chem. Commun.*, 2015, 51, 12467–12469.
- 70 W. Wang, L. B. Fullmer, N. A. G. Bandeira, S. Goberna-Ferrón, L. N. Zakharov, C. Bo, D. A. Keszler and M. Nyman, *Chem*, 2016, 1, 887–901.
- 71 J. L. Bjorklund, M. Shohel, J. W. Bennett, J. A. Smith, M. E. Carolan, E. Hollar, T. Z. Forbes and S. E. Mason, J. Chem. Phys., 2021, 154, 064303.
- 72 M. Shohel, J. L. Bjorklund, E. A. Ovrom, S. E. Mason and T. Z. Forbes, *Inorg. Chem.*, 2020, **59**, 10461–10472.
- 73 M. Shohel, J. L. Bjorklund, J. A. Smith, D. V. Kravchuk, S. E. Mason and T. Z. Forbes, *Angew. Chem., Int. Ed.*, 2021, 60, 8755–8759.
- 74 W. Zhou, N. Ogiwara, Z. Weng, C. Zhao, L. Yan, Y. Kikukawa and S. Uchida, *Chem. Commun.*, 2022, **58**, 12548–12551.
- 75 Y.-F. Sun, Y.-J. Liu, S.-T. Wang, X.-Y. Liu, C. Ma, W.-H. Fang and J. Zhang, *Sci. China Chem.*, 2023, **66**, 1384–1393.

76 S. Yao, W. H. Fang, Y. Sun, S. T. Wang and J. Zhang, J. Am. Chem. Soc., 2021, 143, 2325–2330.

Chemical Science

- 77 H. Xu, Y. Wu, L. Yang, Y. Rao, J. Wang, S. Peng and Q. Li, *Angew. Chem., Int. Ed.*, 2023, **62**, e202217864.
- 78 Y. Kinoshita, Y. Shimoyama, Y. Masui, Y. Kawahara, K. Arai, T. Motohashi, Y. Noda and S. Uchida, *Langmuir*, 2020, **36**, 6277–6285.
- 79 J. Zhu, L. Wang, J. Wang, F. Wang, M. Tian, S. Zheng, N. Shao, L. Wang and M. He, ACS Nano, 2020, 14, 15306– 15316.
- 80 K. W. Corum, M. Fairley, D. K. Unruh, M. K. Payne, T. Z. Forbes and S. E. Mason, *Inorg. Chem.*, 2015, 54, 8367–8374.
- 81 J.-H. Son, H. Choi and Y.-U. Kwon, *J. Am. Chem. Soc.*, 2000, **122**, 7432–7433.
- 82 J.-H. Son and Y.-U. Kwon, *Inorg. Chem.*, 2004, 43, 1929–1932.
- 83 J.-H. Son and Y.-U. Kwon, *Inorg. Chim. Acta*, 2005, **358**, 310–314.
- 84 C.-H. Liu, W.-H. Fang, Y. Sun, S. Yao, S.-T. Wang, D. Lu and J. Zhang, *Angew. Chem., Int. Ed.*, 2021, **60**, 21426–21433.
- 85 B. Achenbach, E. S. Grape, M. Wahiduzzaman, S. K. Pappler, M. Meinhart, R. Siegel, G. Maurin, J. Senker, A. K. Inge and N. Stock, *Angew. Chem., Int. Ed.*, 2023, 62, e202218679.
- 86 Y. Kinoshita, R. Osuga, J. N. Kondo, Y. Ogasawara and S. Uchida, *Chem. Lett.*, 2018, 47, 668–670.
- 87 J. Q. Jiang and N. J. D. Graham, *Environ. Technol.*, 1996, 17, 937–950.
- 88 R. C. Turner, Can. J. Chem., 1969, 47, 2521-2527.
- 89 N. Parthasarathy and J. Buffle, Water Res., 1985, 19, 25-36.
- 90 Z. Wu, X. Zhang, C. Zhou, J. Pang and P. Zhang, RSC Adv., 2016, 6, 108369–108374.
- 91 Z. Chen, B. Fan, X. Peng, Z. Zhang, J. Fan and Z. Luan, *Chemosphere*, 2006, **64**, 912–918.
- 92 M. Shohel, J. A. Smith, M. A. Carolan and T. Z. Forbes, *ACS EST Water*, 2021, 2, 22–31.
- 93 N. Ogiwara and S. Uchida, Chem Catal., 2023, 3, 100607.
- 94 K. Mizuno, T. Mura and S. Uchida, *Cryst. Growth Des.*, 2016, **16**, 4968–4974.
- 95 K. Wen, J. Zhu, H. Chen, L. Ma, H. Liu, R. Zhu, Y. Xi and H. He, *Langmuir*, 2019, **35**, 382–390.
- 96 W. Zhou, N. Ogiwara, Z. Weng, N. Tamai, C. Zhao, L. K. Yan and S. Uchida, *Chem. Commun.*, 2021, 57, 8893–8896.
- 97 Y. J. Liu, H. F. Su, Y. F. Sun, S. T. Wang, C. Y. Zhang, W. H. Fang and J. Zhang, *Angew. Chem.*, *Int. Ed.*, 2023, 62, e202309971.
- 98 E.-M. Han, R.-X. Meng, Y.-Q. Tian, J. Yan, K.-Y. Liu and C. Liu, *Chem. Commun.*, 2023, **59**, 11097–11100.
- 99 M. Muñoz, G. Romanelli, I. L. Botto, C. I. Cabello, C. Lamonier, M. Capron, P. Baranek, P. Blanchard and E. Payen, Appl. Catal., B, 2010, 100, 254–263.

- 100 Y. Cardona, S. A. Korili and A. Gil, Appl. Clay Sci., 2021, 203, 105996.
- 101 S. Wang, S. Li, R. Shi, X. Zou, Z. Zhang, G. Fu, L. Li and F. Luo, *Dalton Trans.*, 2020, 49, 2559–2569.
- 102 Y. Yang, J. Yin, F. Tao, Y. Zhou, L. Zhang, Y. Zhong and Y. Wang, *RSC Adv.*, 2022, **12**, 20251–20258.
- 103 J. Yu, Q. Gao, L. Zhang, Y. Zhou, Y. Zhong, J. Yin, Y. Zhou, F. Tao and Y. Wang, *Dalton Trans.*, 2020, 49, 8122–8135.
- 104 C. Falaise, A. A. Ivanov, Y. Molard, M. Amela Cortes, M. A. Shestopalov, M. Haouas, E. Cadot and S. Cordier, *Mater. Horiz.*, 2020, 7, 2399–2406.
- 105 X. Chen, Y. F. Sun, X. Wu, S. Shi, Z. Wang, J. Zhang, W. H. Fang and W. Huang, *Adv. Mater.*, 2023, 35, e2306260.
- 106 W. Lv, Y. J. Ma, A. N. Wang, Y. Mu, S. W. Niu, L. Wei, W. L. Dong, X. Y. Ding, Y. B. Qiang, X. Y. Li and G. M. Wang, Small, 2024, 20, e2306713.
- 107 S. T. Wang, W. H. Fang and J. Zhang, Angew. Chem., Int. Ed., 2024, 63, e202400161.
- 108 X. Q. Liang, Y. Z. Li, Z. Wang, S. S. Zhang, Y. C. Liu, Z. Z. Cao, L. Feng, Z. Y. Gao, Q. W. Xue, C. H. Tung and D. Sun, *Nat. Commun.*, 2021, 12, 4966.
- 109 Y. Shichibu and K. Konishi, *ChemNanoMat*, 2022, **8**, e202200194.
- 110 D. N. Woodruff, R. E. Winpenny and R. A. Layfield, *Chem. Rev.*, 2013, **113**, 5110–5148.
- 111 C. Kato, R. Machida, R. Maruyama, R. Tsunashima, X. M. Ren, M. Kurmoo, K. Inoue and S. Nishihara, *Angew. Chem., Int. Ed.*, 2018, 57, 13429–13432.
- 112 M. Cesario, C. O. Dietrich-Buchecker, J. Guilhem, C. Pascard and J. P. Sauvage, J. Chem. Soc., Chem. Commun., 1985, 244–247.
- 113 J. F. Stoddart, Angew. Chem., Int. Ed., 2017, 56, 11094-11125.
- 114 P. J. Beldon, L. Fábián, R. S. Stein, A. Thirumurugan, A. K. Cheetham and T. Friščić, *Angew. Chem., Int. Ed.*, 2010, **49**, 9640–9643.
- 115 K. Kubota, T. Seo, K. Koide, Y. Hasegawa and H. Ito, *Nat. Commun.*, 2019, **10**, 111.
- 116 A. X. Yan, S. Yao, Y. G. Li, Z. M. Zhang, Y. Lu, W. L. Chen and E. B. Wang, *Chem.–Eur. J.*, 2014, **20**, 6927–6933.
- 117 C. A. Nagasaka, N. Ogiwara, S. Kobayashi and S. Uchida, *Small*, 2023, e2307004.
- 118 Z. Zhang, Y. Zhu, H. Asakura, B. Zhang, J. Zhang, M. Zhou, Y. Han, T. Tanaka, A. Wang, T. Zhang and N. Yan, *Nat. Commun.*, 2017, **8**, 16100.
- 119 B. Liu, D. Cheng, H. Zhu, J. Du, K. Li, H. Y. Zang, H. Tan, Y. Wang, W. Xing and Y. Li, *Chem. Sci.*, 2019, **10**, 556–563.
- 120 S. Horiuchi, F. Ishii, R. Kumai, Y. Okimoto, H. Tachibana, N. Nagaosa and Y. Tokura, *Nat. Mater.*, 2005, 4, 163–166.